

# Studies on structural, mechanical and erosive wear properties of ZA-27 alloy-based micro-nanocomposites

Proc IMechE Part L  
*J Materials: Design and Applications*  
 0(0) 1–10  
 © IMechE 2021  
 Article reuse guidelines:  
[sagepub.com/journals-permissions](http://sagepub.com/journals-permissions)  
 DOI: 10.1177/1464420721994870  
[journals.sagepub.com/home/pil](http://journals.sagepub.com/home/pil)



Aleksandar Vencel<sup>1,2</sup> , Mara Kandeveva<sup>2,3</sup>, Elena Zadorozhnaya<sup>2</sup>, Petr Svoboda<sup>4</sup> , Michal Michalec<sup>4</sup> , Aleksandar Milivojević<sup>4</sup> and Uroš Trdan<sup>5</sup>

## Abstract

Metal matrix nanocomposites represent a relatively new class of material, which is still being extensively investigated. Most of the studies, however, are devoted to aluminium- or magnesium-based nanocomposites. A limited number of studies focus on zinc alloy base nanocomposites, with fewer still concentrating on zinc alloy base micro-nanocomposites. In addition, most of the tribological studies investigate adhesive or abrasive wear resistance, whereas studies of erosive wear resistance lag well behind. It was previously shown that the presence of nanoparticles in ZA-27 alloy-based nanocomposites led to a slight increase in erosive wear resistance. Upon discovering that, the aim became to produce micro-nanocomposites that would retain the positive effect of nanoparticles, while further elevating performance, by combining microparticles with nanoparticles. The ZA-27 alloy-based micro-nanocomposites were reinforced with 3 wt. % Al<sub>2</sub>O<sub>3</sub> microparticles (particle size approx. 36 μm) and with four different amounts (0.3, 0.5, 0.7 and 1 wt. %) of Al<sub>2</sub>O<sub>3</sub> nanoparticles (particle size 20–30 nm). Tested materials were produced by the compocasting process, with mechanical alloying pre-processing. Solid particle erosive wear testing, with particle impact angle of 90°, showed that all micro-nanocomposites had significantly increased wear resistance in comparison to the reference material.

## Keywords

ZA-27 alloy, micro-nanocomposites, compocasting, microstructure, hardness, erosive wear

Date received: 18 December 2020; accepted: 26 January 2021

## Introduction

In recent years, extensive research efforts have been made to develop nanocomposite materials by using different ingot metallurgy (casting) processes. Most of these studies were related to the development of nanocomposites with an aluminium<sup>1–3</sup> or magnesium<sup>4,5</sup> alloy base, and the addition of ceramic nanoreinforcements. There are significantly fewer studies focused on nanocomposites with a zinc alloys base,<sup>6–9</sup> even though there are numerous research activities related to development of such microcomposites.<sup>10–12</sup> The most frequently used zinc alloy base is ZA-27, a zinc-aluminium alloy, that contains a relatively high aluminium content,<sup>13</sup> while during the production of microcomposites different secondary phases were used, e.g. SiC, Al<sub>2</sub>O<sub>3</sub> and other ceramic particles,<sup>10–12</sup> graphite particles<sup>14</sup> as well as short glass fibres.<sup>15</sup>

The ZA-27 alloy is a commercial casting alloy, which can be found in a wide range of applications, particularly in the automotive industry due to its high

strength to weight ratio.<sup>16</sup> It has been frequently used in the production of sliding bearings and bushings because of its relatively high adhesive wear resistance.<sup>17</sup> Wide solidification interval, between liquidus and solidus temperature, allows processing of ZA-27 alloy in the semi-solid state,<sup>18</sup> i.e. production of the composites with ZA-27 alloy base by the

<sup>1</sup>University of Belgrade, Faculty of Mechanical Engineering, Belgrade, Serbia

<sup>2</sup>South Ural State University, Chelyabinsk, Russia

<sup>3</sup>Faculty of Industrial Technology, Technical University of Sofia, Sofia, Bulgaria

<sup>4</sup>Faculty of Mechanical Engineering, Brno University of Technology, Brno, Czech Republic

<sup>5</sup>Faculty of Mechanical Engineering, University of Ljubljana, Ljubljana, Slovenia

### Corresponding author:

Aleksandar Vencel, University of Belgrade, Faculty of Mechanical Engineering, Kraljice Marije 16, 11120 Belgrade, Serbia.  
 Email: [avencel@mas.bg.ac.rs](mailto:avencel@mas.bg.ac.rs)

compocasting process.<sup>19</sup> The compocasting process permits the production of economical and quality metal matrix composites (MMCs) with a non-dendritic matrix structure. This process is carried out at substantially lower temperatures compared to the e.g. high-pressure die casting, thereby generating energy savings, lowering emissions, and extending tool life. In addition, it is possible to obtain near net shape castings that can be later processed by stir casting, squeeze casting<sup>20</sup> or by extrusion.<sup>21</sup>

Nowadays, the compocasting process is also used to produce metal matrix nanocomposites (MMnCs). The addition of nanoparticles in MMnCs lead to the beneficial increase of both strength and ductility compared to the metal matrix. This is unlike MMCs, where the strength increase is accompanied by a decrease in ductility (compared to the matrix alloy). In order to further improve the properties of MMCs and/or MMnCs, research activities have also been focused on the production of composite materials that contain both micro- and nanoparticles.<sup>22,23</sup> Despite considerable progress in this area, little attention has been paid to the production and characterization of zinc alloys-based micro-nanocomposites. Hence, the aim of this paper was to investigate the production possibility of various ZA-27 alloy-based micro-nanocomposites through the compocasting process, as well as to analyse structural, mechanical and erosive wear properties of the obtained composites.

## Experimental details

### Materials

Matrix material was zinc-aluminium alloy ZA-27, with the chemical composition according to the ASTM standard.<sup>13</sup> Type, size and amount of reinforcement particles used for obtaining of the micro-composite and micro-nanocomposites are shown in Table 1. The investigated microcomposite (composite with the addition of Al<sub>2</sub>O<sub>3</sub> microparticles only) was produced by the compocasting process on the apparatus, which is described elsewhere.<sup>24</sup> Micro-nanocomposites (composites with the addition of Al<sub>2</sub>O<sub>3</sub> microparticles and Al<sub>2</sub>O<sub>3</sub> nanoparticles) were produced using the same process and apparatus,

whereas the mechanical alloying of ceramic nanoparticles with ZA-27 alloy metal chips were applied beforehand. It was applied in order to reduce the formation of the Al<sub>2</sub>O<sub>3</sub> nanoparticle cluster agglomerations in the matrix. Before this pre-processing, the ZA-27 alloy metal chips were thoroughly washed in trichloroethylene and then in ethanol for degreasing, while the Al<sub>2</sub>O<sub>3</sub> nanoparticles were washed in ethanol before and heated to 400°C in order to remove the moisture and contaminations. The mechanical alloying parameters were similar as in our previous study.<sup>25</sup> The only difference is in metal chips-to-nanoparticles weight ratio (2:1 vs. 3:1). After mechanical alloying, the mixture of ZA-27 alloy metal chips and Al<sub>2</sub>O<sub>3</sub> nanoparticles was mixed with Al<sub>2</sub>O<sub>3</sub> microparticles. The resulting mixture was homogenized for 60 min in a mixer without alumina balls.

The compocasting process started with the matrix alloy overheating at 550°C and cleaning of the slag. Afterwards, the temperature of the melt was reduced to 500°C, followed by mixing the melt with a stirrer at 250 r/min. Infiltration of the mixture, obtained in mechanical alloying process, started at this temperature and lasted for 3 min. After the infiltration, mixing of the melt at increased rate of 500 r/min lasted for 5 min. With continued mixing, the temperature of the melt was reduced further to 465°C (cooling rate of 5°C/min). Additional mixing at this temperature was continued for 8 min, after which the melt was poured into a preheated steel mould (at 480°C). Reference material was ZA-27 alloy, produced by thixocasting (designated as ZA-TX). For the purpose of comparison, the parameters of the thixocasting and compocasting process were kept similar. The matrix alloy was first overheated at 550°C, and the slag was cleaned. After that, the temperature of the melt was reduced to 500°C, followed by mixing of the melt with a stirrer at 500 r/min, for 5 min. Then, with continued mixing, the temperature of the melt was reduced further to 465°C (cooling rate of 5°C/min). Additional mixing at this temperature was continued for 8 min, after which the melt was poured into a preheated steel mould (at 480°C). At the end of the producing process, all samples (ZA-TX, as well as composites samples) were hot-pressed (350°C and 250 MPa).

### Methods of characterization

Plate-like samples (15 × 15 × 6 mm) were postulated for microstructural examinations on the scanning electron microscopy (SEM). Prior to SEM observations, the sample surfaces were successively grinded with the P80, P360 and P600 grit SiC abrasive papers and afterwards polished with paste containing Al<sub>2</sub>O<sub>3</sub> microparticles (particle size 1–5 µm). Hardness measurements (Vickers macro- and microhardness) were performed on plate-like samples (30 × 15 × 6 mm) that were used for erosive wear tests. Macrohardness (HV 5) was

**Table 1.** Designation of the produced composites and specification of used reinforcements.

Composite designation	Reinforcement amount, wt. %	
	Al <sub>2</sub> O <sub>3</sub> microparticles (approx. 36 µm)	Al <sub>2</sub> O <sub>3</sub> nanoparticles (20–30 nm)
Micro	3	–
MN-0.3		0.3
MN-0.5		0.5
MN-0.7		0.7
MN-1.0		1.0

determined for the purpose of comparison with our previous studies,<sup>26,27</sup> while the microhardness (HV 0.5) was determined in order to diminish the influence of porosity and other defects. For each material, measurements of both hardness were repeated at least five times and an average value with a standard deviation was calculated to obtain reproducibility of the results.

Erosive wear tests were carried out on plate-like samples ( $30 \times 15 \times 6$  mm), using the jet nozzle type solid particle erosion equipment, and exposed to air, at room conditions. Detailed description of the apparatus and the test procedure are presented elsewhere.<sup>25,28</sup> Parameters used in the erosive wear testing were the same for all tested samples (Table 2), and, for the purpose of comparison, the same as in our previous study.<sup>25</sup> Used solid particles had sharp edges and irregular morphology, and they were dried in an oven before the tests to remove any remaining moisture. Wear was calculated as a difference between the initial mass of the sample and its mass at the end of the test. For this purpose, electronic balance with accuracy of 0.1 mg was used. Calculation of the wear rate was done by dividing mass loss of the sample material by the mass of applied solid particles material during the test, which was 500 g. Cleaning and degreasing of the

samples were done before and after the testing. At least three replicate tests were performed for each material. Worn surfaces of samples were analysed with SEM, after the testing.

## Results and discussion

### Microstructure

The microstructure of the thixocasted ZA-27 alloy is non-dendritic, and regions of  $\alpha$  phase (dark gray areas),  $\alpha + \eta$  phase mixture (middle gray areas) and  $\eta$  phase (light gray areas) can be noticed (Figure 1). The regions of  $\alpha$  phase and  $\alpha + \eta$  phase mixture form elliptical microconstituents. Transformation of dendritic to non-dendritic structure occurred under the influence of shear forces during mixing of the ZA-27 alloy semi-solid melt. According to the Al-Zn phase diagram,<sup>16</sup> solidification of conventional cast ZA-27 alloy begins with the formation of  $\alpha$  phase nuclei. The growth of the nuclei in the melt during solidification results in formation of  $\alpha$  phase particles. At peritectic temperature, the  $\alpha$  phase particles (dendrites) react with the melt, and high temperature  $\beta$  phase is formed at edges of the  $\alpha$  phase particles. The  $\beta$  phase is unstable at lower temperatures.<sup>29</sup> During further cooling, the  $\beta$  phase transforms into the  $\alpha + \eta$  phase mixture so that the  $\alpha$  phase and the  $\alpha + \eta$  phase mixture form a dendritic shape microconstituents.

In the conventionally casted structure, when the process of solidification takes place without the influence of external forces, the  $\alpha$  phase forms the dendrite cores, while the  $\alpha + \eta$  phase mixture is present in the proximity of dendrites. The  $\eta$  phase is the interdendritic phase. Due to the influence of shear forces during mixing (thixocasting process), the  $\alpha$  phase (dendrites) are transformed into a non-dendritic

**Table 2.** Parameters used in the erosive wear testing.

Test parameter	Value
Solid particles material	Black corundum ( $\text{Al}_2\text{O}_3$ )
Maximum size of the particles	630 $\mu\text{m}$
Air stream pressure	0.2 MPa
Particles flow	167 g/min
Particles impact angle	90°
Distance between the sample and the nozzle	10 mm
Duration of the test	3 minutes

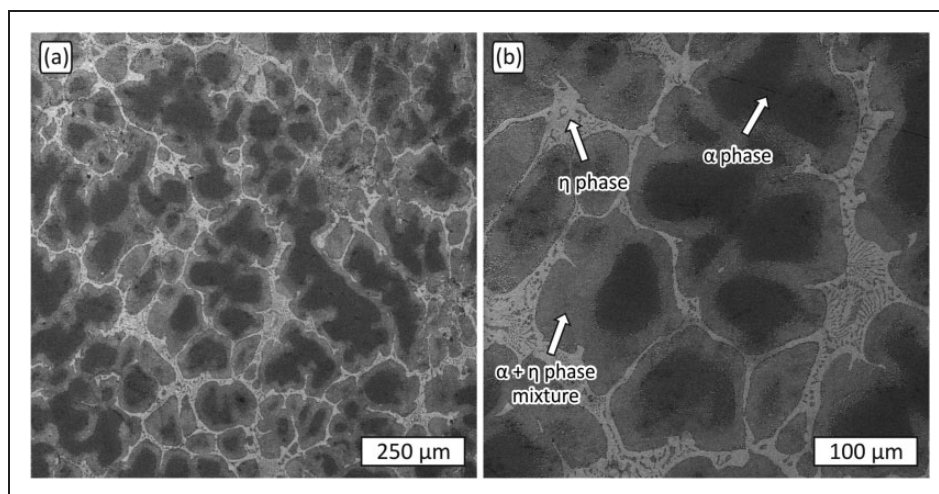


**Figure 1.** Microstructure of thixocasted ZA-27 alloy, SEM: (a) general view and (b)  $\alpha$  phase formed by deagglomeration of large  $\alpha$  phase region.



shape (deformed ellipses). During the thixocasting process, the cooling time of the semi-solid melt in the preheated mould was longer, which resulted in a prolonged peritectic reaction and expanded regions of  $\alpha + \eta$  phase mixtures (Figure 1). Agglomeration and deagglomeration of primary particles of the solid phase occur under the influence of shear forces during mixing of semi-solid melts.<sup>30</sup> Large regions of  $\alpha$  phase that are formed by agglomeration of smaller elliptic  $\alpha$  phase regions can be seen in Figure 1(a), while regions of  $\alpha$  phase formed by deagglomeration of large  $\alpha$  phase region are clearly visible in Figure 1(b).

Microstructures of all micro-nanocomposites were very similar (Figures 2 and 3). General view of the microstructure (Figure 2(a)) confirms that the  $\text{Al}_2\text{O}_3$  microparticles are placed in the regions of  $\alpha + \eta$  phase mixture, and that the structure of micro-nanocomposites matrix is the same as the structure of thixocasted ZA-27 alloy. The distribution of  $\text{Al}_2\text{O}_3$  microparticles (particle size approx.  $36\ \mu\text{m}$ ) is analysed on higher magnification image (Figure 2(b)). A good mechanical bonding between the incorporated  $\text{Al}_2\text{O}_3$  microparticles and the metal matrix, with low content of porosity and without contact between the particles, was obtained. This is very significant for achieving good mechanical properties, as well as high erosive wear resistance. Groups of  $\text{Al}_2\text{O}_3$  nanoparticle clusters (denoted with white arrows) can also be noticed on Figure 2(b).

The distribution of  $\text{Al}_2\text{O}_3$  nanoparticles (particle size 20–30 nm) is analysed on higher magnification images (Figure 3). The  $\text{Al}_2\text{O}_3$  nanoparticles are present in the form of agglomerated (Figures 3(a) and (b)) or mostly uniform distribution of clusters (Figure 3(c)). The presence of significant microporosity in the structure of micro-nanocomposites is not visible, although micropores can be noticed near some  $\text{Al}_2\text{O}_3$  microparticles. There is no strict relationship between the amount of  $\text{Al}_2\text{O}_3$  nanoparticles and microstructure of the produced micro-nanocomposites, i.e. the structure

mainly depends on the production parameters and their control.

Example of  $\text{Al}_2\text{O}_3$  nanoparticles agglomeration, composed of several small and large clusters, is clearly visible on Figure 3(a) (denoted with white arrow). These agglomerations and  $\text{Al}_2\text{O}_3$  nanoparticle clusters are mainly randomly distributed within the microstructure. Sometimes, they are placed between ceramic microparticles (Figure 3(b)), which may prevent appropriate bonding between the microparticles and the matrix. In some cases, the presence of cracks in ceramic microparticles is also evident (denoted with rectangle on Figure 3(b)). These microcracks probably appeared due to thermal stresses, which occurred during the cooling of the composite mixture. Their presence adversely affects the mechanical and erosive wear properties of the produced micro-nanocomposites. On the other hand, uniform distribution of the  $\text{Al}_2\text{O}_3$  nanoparticle clusters and their favourable shape and size should have a positive effect. Such example can clearly be observed in Figure 3(c) (denoted with white arrow), where  $\text{Al}_2\text{O}_3$  nanoparticles clusters are circular, with size up to  $2\ \mu\text{m}$ , and uniformly distributed within the  $\alpha + \eta$  phase mixture.

### Hardness

The macro- and microhardness results presented in Figures 4 and 5 confirm good repeatability of the results, when calculated standard deviations were below 8%. The presented hardness values are lower than that obtained in our previous studies.<sup>26,27</sup> Also, the prescribed values of hardness for sand/die cast ZA-27 alloy are 113/119 HB.<sup>13</sup> Relatively lower hardness was probably obtained due to the increase in the preheating temperature of the steel mould (from 400 to  $480^\circ\text{C}$ ), and associated longer cooling time and smaller cooling rate of the samples. A change in the composting process in the mixing part could lead to loss of magnesium, which also could have a diminishing effect on the hardness. As expected and as showed

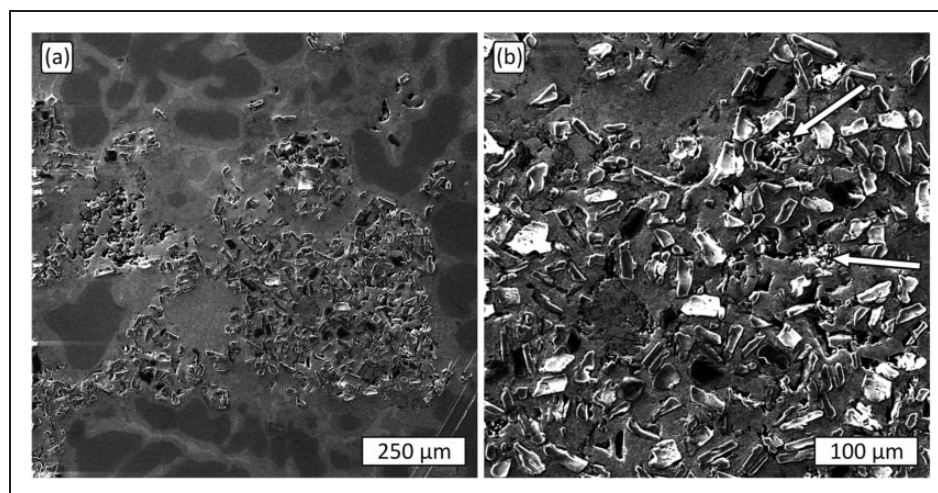


**Figure 2.** Microstructure of micro-nanocomposite MN-0.3, SEM: (a) general view, (b) microparticles distribution.

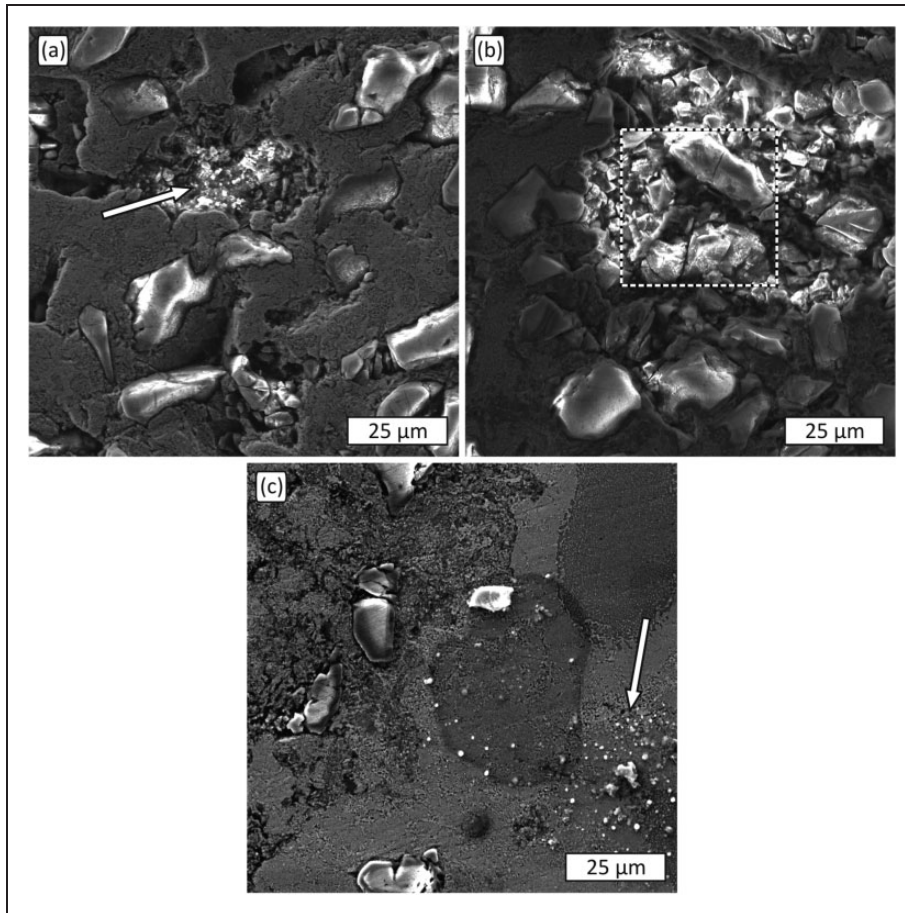


**Figure 3.** Microstructure of micro-nanocomposites (nanoparticle clusters distribution), SEM: (a) micro-nanocomposite MN-0.3, (b) micro-nanocomposite MN-0.5 and (c) micro-nanocomposite MN-1.0.

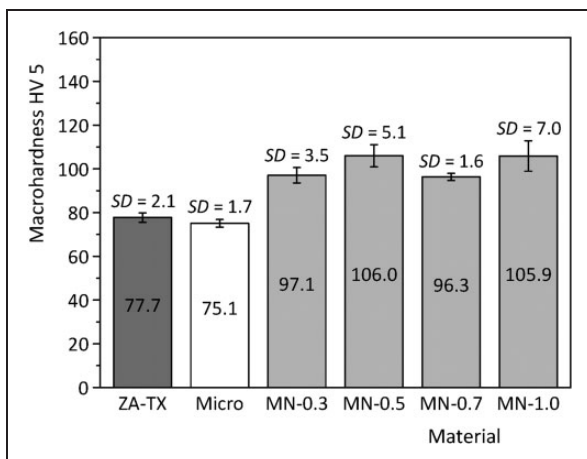


**Figure 4.** Macrohardness values and corresponding standard deviations (SD) of tested materials.

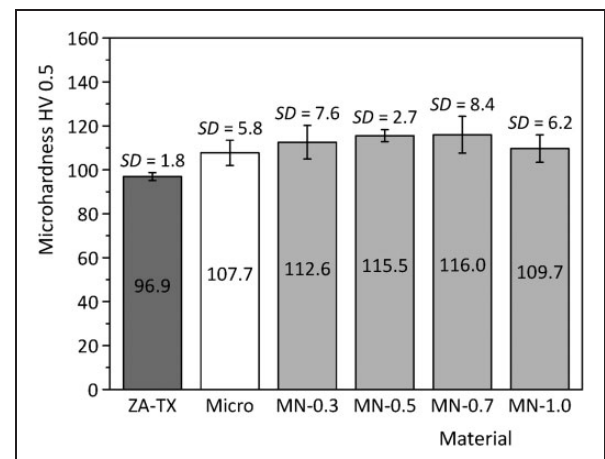


**Figure 5.** Microhardness values and corresponding standard deviations (SD) of tested materials.

in some previous studies,<sup>31,32</sup> microhardness values, which were measured with lower load, were slightly higher than macrohardness values.

All micro-nanocomposites achieved more-or-less similar hardness values, which were expected due to their similar microstructures. Although a higher

amount of nanoparticles should result in higher hardness of the nanocomposites,<sup>11</sup> it should be noted that the hardness of composites also strongly depends on the interface between reinforcements and matrix as well as on distribution of the reinforcements.<sup>33</sup> The positive effect of a higher amount of nanoparticles on

hardness diminishes with higher content of porosity. Microstructural examinations have confirmed favourable distribution of micro- and nanoparticles in the micro-nanocomposite with the lowest amount of the nanoparticles. The agglomerations of nanoparticle clusters are placed in the regions between the microparticles and contact between the nanoparticles and microparticles were not detected (Figure 3(a)). Hence, lower porosity was achieved. On the other hand, a higher amount of nanoparticles caused increased agglomeration of nanoparticle clusters, which were in contact with microparticles (Figure 3 (b)). Contact between the nanoparticles and microparticles led to the discontinuity of the microparticle/matrix interface, which adversely affected the load transfer from the matrix to the reinforcements, thereby decreasing the hardness. In addition, microcracks within the microparticles were also noticed. Regardless of the nanoparticle amount, all micro-nanocomposites achieved higher hardness than thixocasted ZA-27 alloy. The average percentage increase of macrohardness was around 30%, which is much higher than when only nanoparticles were incorporated in the matrix alloy (around 9%).<sup>26,27</sup> This is probably due to the combination of different reinforcement mechanisms, i.e. difference in coefficients of thermal expansion (microparticles) and Orowan dislocation strengthening mechanism (nanoparticles).

### Erosive wear properties

The wear rate results of the tested materials obtained by erosive wear testing are shown in Figure 6. The standard deviation values of the erosive wear rates indicate that the repeatability of the results was acceptable, i.e. around 10%. The wear rate of thixocasted ZA-27 alloy (ZA-TX) is like the one obtained in our previous study,<sup>25</sup> although the hardness of the same material in that study was higher. This can be explained by the fact that the hardness is directly related to the erosive wear rate, but only to be applied

for annealed pure metals, when small impact angles are applied.<sup>34</sup> Indeed, erosion is a complex phenomenon. For ductile metals, it is impossible to use a single mechanical property or a simple combination of a few mechanical properties to predict its erosive wear resistance.<sup>35</sup>

Results in Figure 6 clearly depict that the highest wear rate was obtained with the microcomposite material (composite with the addition of 3 wt.%  $\text{Al}_2\text{O}_3$  microparticles only). Although this composite had similar hardness as the thixocasted ZA-27 alloy, its wear rate was slightly higher and could be increased with a higher amount of  $\text{Al}_2\text{O}_3$  microparticles, especially because a harder MMCs can show higher erosion wear than a softer material.<sup>36</sup> Although MMCs mostly experience higher abrasive and adhesive wear resistance than the matrix material,<sup>37,38</sup> their erosive wear behaviour is less predictable. Moreover, it has been shown that the erosive wear resistance of the aluminium alloy-based composites, carbide-metal composites, cermets, nickel-chromium superalloy composites and steel-based composites is often lower than that of the matrix material.<sup>35,39–41</sup> Reduced erosive wear resistance of the MMCs reinforced with higher amount of micro-sized ceramic particles is usually connected with significant lowering of the ductility. Hence, lower ductility results in reduced plastic deformation ability, which enhances the possibility of microfracture upon impact of the erosive particles.<sup>42</sup>

All micro-nanocomposites (composites with the addition of  $\text{Al}_2\text{O}_3$  microparticles and  $\text{Al}_2\text{O}_3$  nanoparticles) showed a lower wear rate than the thixocasted ZA-27 alloy. The average reduction of the wear rate compared to the reference material was in this case relatively high, i.e. 53%. This suggests that the simultaneous addition of micro- and nanoparticles had a major, beneficial effect on the erosive wear rate. This is most likely associated with the collateral effect of the dual, i.e. micro- and nanoparticles reinforcement of the matrix material. Introducing additional micro- or nanoparticles separately does not show a strong influence on erosive wear rate reduction. For example, the addition of  $\text{Al}_2\text{O}_3$  nanoparticles reduces wear rate only by approximately 6%,<sup>25</sup> while the addition of  $\text{Al}_2\text{O}_3$  microparticles increases the erosive wear rate even more (Figure 6). In our previous study,<sup>26</sup> it was shown that the adding of  $\text{Al}_2\text{O}_3$  nanoparticles somehow increases hardness and compressive yield strength through the enhanced dislocation density strengthening mechanism. It is highly likely that the addition of nanoparticles also increase the ductility of micro-nanocomposites, which seems to be reflected during the erosive wear testing with particles at an impact angle of  $90^\circ$ . This property combined with the increased strength (due to the presence of ceramic microparticles) resulted in a lower wear rate of micro-nanocomposites. The results of this study confirm similar wear rates for all micro-nanocomposites,

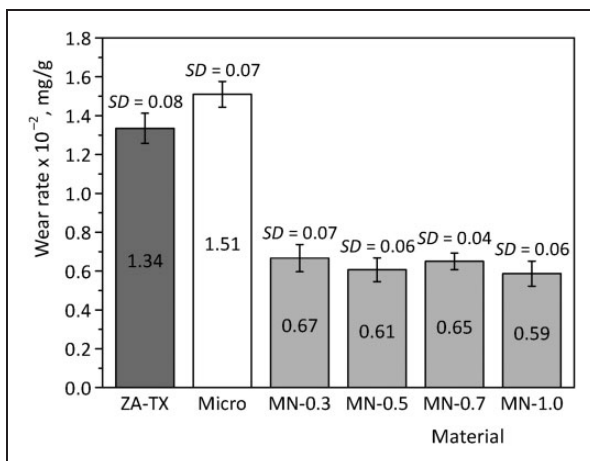


**Figure 6.** Erosive wear rate values and corresponding standard deviations (SD) of tested materials.



which are reflected in the obtained microstructures and overall hardness. Theory suggests that the wear rate should be lower in micro-nanocomposites with a higher number of nanoparticles; however, this is not the case. This is mainly due to the structural imperfections that were noticed in all micro-nanocomposites (Figures 2 and 3). The poor distribution of nanoparticles (agglomerations of clusters) and positioning around microparticles, as well as the presence of cracked microparticles had a detrimental effect on the erosive wear rate/resistance.

The SEM analyses of worn surfaces (depicted in Figure 7), which were performed after testing, showed typical erosive wear appearance in all worn surfaces.<sup>43</sup> This generally includes several erosive wear mechanisms that usually occur simultaneously, i.e. microcutting and microploughing; surface cracking; extrusion of material at the exit of impact crater; surface or subsurface fatigue cracks due to the repeated impact; formation of thin platelets due to the extrusion and forging by repeated impact and formation of platelets by a backward extrusion process.<sup>34</sup> The plastic deformation in the surface of the extruded material around the large indents and its smearing by subsequent impacts of particles, presence of scratches

and grooves caused by the ploughing action of particles which additionally caused progressive degradation of the surface with small and large wear debris, can be observed in all samples. However, a greater presence of surface cracks and the presence of embedded erosive particles were not noticed. The relatively large size of the erosive particles ( $\leq 630 \mu\text{m}$ ) and other test parameters prevented the embedment of the erosive particles.

The differences in the appearance of the worn surface between tested materials are, first of all, in the severity of plastic deformation. This severity was more intensive in thixocasted ZA-27 alloy and micro-composite. Furthermore, the presence of relatively large wear debris and surface microcracks is also observed on the worn surface of thixocasted ZA-27 alloy (Figure 7(a)). The formation of plastically deformed and extruded material is noticeable around the large indents (craters). There are also some small indents and scratches, which most likely occurred during the impact of small and sharp erosive particles or its fragments (microcutting). In micro-composites, in comparison to thixocasted ZA-27 alloy, the indents on the worn surface are more massive in size (Figure 7(b)). Also, the presence of large

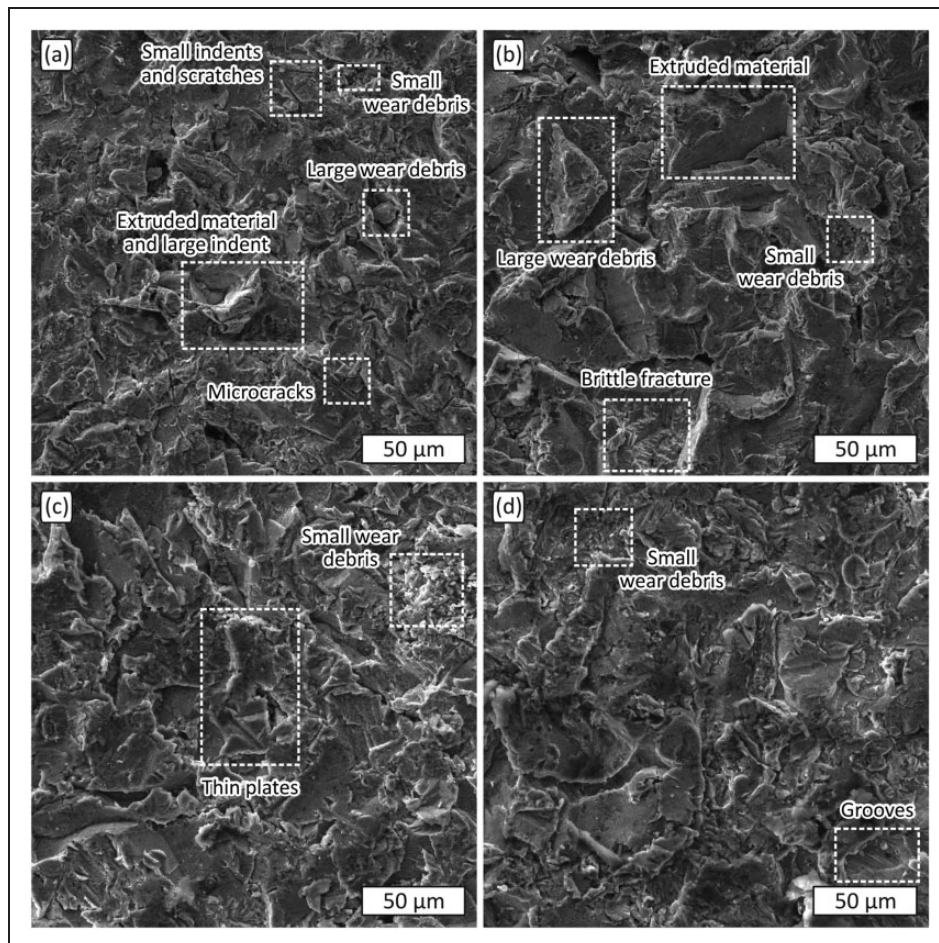


**Figure 7.** Worn surfaces of tested materials, SEM: (a) thixocasted ZA-27 alloy, (b) microcomposite, (c) micro-nanocomposite MN-0.3 and (d) micro-nanocomposite MN-1; all images are taken with the same magnification (1000 $\times$ ).

wear debris in the form of plates and even brittle fractures is only noticeable on the worn surface of the microcomposite.

The worn surfaces of all micro-nanocomposites were very similar (Figure 7(c) and (d)). This is consistent with the wear rates of these composites (Figure 6), where similar values were recorded. In contrast to thixocasted ZA-27 alloy and microcomposite, no large wear debris was observed on their worn surfaces. On the other hand, the presence of thin plates and grooves caused by the ploughing action of erosive particles and ductile fracture (microploughing) was noticed only on the worn surfaces of micro-nanocomposites. The formation of thin plates can be identified as one of the previously mentioned erosive wear mechanism,<sup>34</sup> i.e. as “formation of thin platelets due to the extrusion and forging by repeated impact.” Furthermore, since the particles impact angle was 90°, it can be concluded that plastic deformation and work hardening of the thin surface layer, with induced compressive residual stresses, occurred.<sup>42</sup> All of this provides a possible explanation for the significantly higher erosive wear resistance of all micro-nanocomposites, compared to the thixocasted ZA-27 alloy and microcomposite.

## Conclusions

In order to reduce the undesired formation of nanoparticle clusters in the matrix alloy, mechanical alloying of ceramic nanoparticles with a scrap of the matrix alloy was applied before the compocasting process. Through this process, complex microparticles, more suitable for infiltration in the semi-solid matrix alloy during the compocasting process, were formed.

Microstructures of all micro-nanocomposites were similar, i.e. there was no obvious relationship between the amount of Al<sub>2</sub>O<sub>3</sub> nanoparticles and the microstructure of the produced micro-nanocomposites. The Al<sub>2</sub>O<sub>3</sub> nanoparticles appeared in the form of relatively uniformly distributed clusters. In most cases, these clusters were not in direct contact with Al<sub>2</sub>O<sub>3</sub> microparticles, which would prevent the appropriate bonding between the microparticles and the matrix. This is an important feature for obtaining good mechanical properties and higher erosive wear resistance. All micro-nanocomposites achieved similar hardness values. Regardless the number of nanoparticles, the hardness of micro-nanocomposites was higher than that of the thixocasted ZA-27 alloy. The average percentage increase of macrohardness was around 30%.

All micro-nanocomposites achieved similar erosive wear resistance, which was much higher than that of thixocasted ZA-27 alloy. The average reduction of wear rate was 53%. Higher erosive wear rates were obtained due to the dual effect of simultaneously added micro- and nanoparticles. It is likely that microparticles led to increased strength, while nanoparticles

prevented the lowering of ductility of the matrix material, potential even causing an increase. In addition, SEM analyses showed that micro-nanocomposites had a specific worn surface appearance, suggesting that forging by repeated impact and work hardening of the surface most likely had occurred.




## Declaration of conflicting interests

The author(s) declared no potential conflicts of interest with respect to the research, authorship, and/or publication of this article.

## Funding

The author(s) disclosed receipt of the following financial support for the research, authorship, and/or publication of this article: This work has been performed as a part of activities within the project 451-03-68/2020-14/200105, supported by the Republic of Serbia, Ministry of Education, Science and Technological Development, and its financial help is gratefully acknowledged. Mara Kandeve acknowledges the project ДН 07/28-15.12.2016, funded by the National Science Fund of the Ministry of Education and Science, Bulgaria. Petr Svoboda and Michal Michalec acknowledge the project FSI-S-17-4415, funded by the Ministry of Education, Youth and Sports of Czech Republic. Uroš Trdan acknowledges the financial support from the state budget by the Slovenian Research Agency Programme No. P2-0270. Collaboration through the CEEPUS network CIII-BG-0703, COST action CA15102 and bilateral Project 337-00-00111/2020-09/50 and BI-RS/20-21-047 between Republic of Serbia and Republic of Slovenia is also acknowledged.

## ORCID iDs

Aleksandar Vencl  <https://orcid.org/0000-0002-2208-4255>  
Petr Svoboda  <https://orcid.org/0000-0003-3091-4025>  
Michal Michalec  <https://orcid.org/0000-0002-8803-9043>

## References

1. Sajjadi SA, Torabi Parizi M, Ezatpour HR, et al. Fabrication of A356 composite reinforced with micro and nano Al<sub>2</sub>O<sub>3</sub> particles by a developed compocasting method and study of its properties. *J Alloys Compd* 2012; 511: 226–231.
2. Karbalaee Akbari M, Baharvandi HR and Mirzaee O. Nano-sized aluminum oxide reinforced commercial casting A356 alloy matrix: evaluation of hardness, wear resistance and compressive strength focusing on particle distribution in aluminum matrix. *Compos Part B: Eng* 2013; 52: 262–268.
3. Karbalaee Akbari M, Baharvandi HR and Mirzaee O. Fabrication of nano-sized Al<sub>2</sub>O<sub>3</sub> reinforced casting aluminum composite focusing on preparation process of reinforcement powders and evaluation of its properties. *Compos Part B: Eng* 2013; 55: 426–432.
4. Hassan SF and Gupta M. Development of high performance magnesium nanocomposites using solidification processing route. *Mater Sci Technol* 2004; 20: 1383–1388.
5. Lan J, Yang Y and Li X. Microstructure and microhardness of SiC nanoparticles reinforced magnesium



- composites fabricated by ultrasonic method. *Mater Sci Eng A* 2004; 386: 284–290.
6. Swiderska-Sroda A, Kalisz G, Grzanka E, et al. SiC-Zn nanocomposites obtained using the high-pressure infiltration technique. *Solid State Phenom* 2006; 114: 257–262.
  7. Karimzadeh F, Enayati MH and Tavoosi M. Synthesis and characterization of Zn/Al<sub>2</sub>O<sub>3</sub> nanocomposite by mechanical alloying. *Mater Sci Eng A* 2008; 486: 45–48.
  8. De Cicco MP, Li X and Turng L-S. Semi-solid casting (SSC) of zinc alloy nanocomposites. *J Mater Process Technol* 2009; 209: 5881–5885.
  9. Li ZG. Fabrication of in situ TiB<sub>2</sub> particulates reinforced zinc alloy matrix composite. *Mater Lett* 2014; 121: 1–4.
  10. Sharma SC, Girish BM, Somashekar DR, et al. Sliding wear behaviour of zircon particles reinforced ZA-27 alloy composite materials. *Wear* 1999; 224: 89–94.
  11. Sastry S, Krishna M and Uchil J. A study on damping behaviour of aluminite particulate reinforced ZA-27 alloy metal matrix composites. *J Alloys Compd* 2001; 314: 268–274.
  12. Sharma SC, Sastry S and Krishna M. Effect of aging parameters on the micro structure and properties of ZA-27/aluminite metal matrix composites. *J Alloys Compd* 2002; 346: 292–301.
  13. ASTM B 86:2013. Standard specification for zinc and zinc-aluminum (ZA) alloy foundry and die castings.
  14. Seah KHW, Sharma SC and Girish BM. Mechanical properties of cast ZA-27/graphite particulate composites. *Mater Des* 1995; 16: 271–275.
  15. Sharma SC, Girish BM, Satish BM, et al. Aging characteristics of short glass fiber reinforced ZA-27 alloy composite materials. *J Mater Eng Perform* 1998; 7: 747–750.
  16. Gervais E, Barnhurst RJ and Loong CA. An analysis of selected properties of ZA alloys. *JOM* 1985; 37: 43–47.
  17. Rac A, Babić M and Ninković R. Theory and practice of Zn-Al sliding bearings. *J Balk Tribol Assoc* 2001; 7: 234–240.
  18. Chen TJ, Hao Y and Li YD. Effects of processing parameters on microstructure of thixoformed ZA27 alloy. *Mater Des* 2007; 28: 1279–1287.
  19. Karni N, Barkay GB and Bamberger M. Structure and properties of metal-matrix composite. *J Mater Sci Lett* 1994; 13: 541–544.
  20. Ribes H and Suéry M. Effect of particle oxidation on age hardening of Al-Si-Mg/SiC composites. *Scr Metall* 1989; 23: 705–709.
  21. Rahmani Fard R and Akhlaghi F. Effect of extrusion temperature on the microstructure and porosity of A356-SiC<sub>p</sub> composites. *J Mater Process Technol* 2007; 187–188: 433–436.
  22. Rajmohan T, Palanikumar K and Arumugam S. Synthesis and characterization of sintered hybrid aluminium matrix composites reinforced with nanocopper oxide particles and microsilicon carbide particles. *Compos Part B: Eng* 2014; 59: 43–49.
  23. Karbalaei Akbari M, Baharvandi HR and Shirvanimoghaddam K. Tensile and fracture behavior of nano/micro TiB<sub>2</sub> particle reinforced casting A356 aluminum alloy composites. *Mater Des* 2015; 66A: 150–161.
  24. Vencl A, Bobić I, Jovanović MT, et al. Microstructural and tribological properties of A356 Al-Si alloy reinforced with Al<sub>2</sub>O<sub>3</sub> particles. *Tribol Lett* 2008; 32: 159–170.
  25. Vencl A, Bobić I, Bobić B, et al. Erosive wear properties of ZA-27 alloy-based nanocomposites: influence of type, amount and size of nanoparticle reinforcements. *Friction* 2019; 7: 340–350.
  26. Bobić B, Vencl A, Ružić J, et al. Microstructural and basic mechanical characteristics of ZA27 alloy-based nanocomposites synthesized by mechanical milling and compocasting. *J Compos Mater* 2019; 53: 2033–2046.
  27. Vencl A, Bobić I and Kandeva M. Influence of small addition of nano particles on mechanical and erosive wear properties of zinc-based nanocomposites. In: *International conference on "Trends in Nanotribology 2017" (TiN17)*, Trieste, Italy, 26–30 June 2017, posters.
  28. Vencl A, Kandeva M and Bobić I. Influence of nanoparticles amount on erosive wear properties of ZA-27 alloy-based dual-size composites. In: *1st international conference on technological innovations in metals engineering (TIME)*, Haifa, Israel, 30–31 May 2018, p.48.
  29. Murphy S and Savaskan T. Metallography of zinc-25% Al based alloys in the as-cast and aged conditions. *Pract Metall* 1987; 24: 204–221.
  30. Flemings MC. Behavior of metal alloys in the semisolid state. *Metall Trans A* 1991; 22: 957–981.
  31. Vencl A, Mrdak M and Hvizdos P. Tribological properties of WC-Co/NiCrBSi and Mo/NiCrBSi plasma spray coatings under boundary lubrication conditions. *Tribol Ind* 2017; 39: 183–191.
  32. Vencl A, Vučetić F, Bobić B, et al. Tribological characterization in dry sliding conditions of compocasted hybrid A356/SiC<sub>p</sub>/Gr<sub>p</sub> composites with graphite macroparticles. *Int J Adv Manuf Technol* 2019; 100: 2135–2146.
  33. Rohatgi PK, Liu Y and Ray S. Friction and wear of metal-matrix composites. In: PJ Blau (ed.) *ASM handbook: friction, lubrication, and wear technology* (Volume 18). Metals Park: ASM International, 1992, pp.801–811.
  34. Zum Gahr K-H. *Microstructure and wear of materials*. Amsterdam: Elsevier, 1987.
  35. Liu X. *A study on the erosion and erosion-oxidation of metal matrix composites*. PhD thesis, Helsinki University of Technology, Finland, 2003.
  36. Peat T, Galloway A, Toumpis A, et al. The erosion performance of particle reinforced metal matrix composite coatings produced by co-deposition cold gas dynamic spraying. *Appl Surf Sci* 2017; 396: 1623–1634.
  37. Vencl A. Tribology of the Al-Si alloy based MMCs and their application in automotive industry. In: L Magagnin (ed.) *Engineered metal matrix composites: forming methods, material properties and industrial applications*. New York: Nova Science Publishers, 2012, pp.127–166.
  38. Vučetić F, Veličković S, Milivojević A, et al. A review on tribological properties of microcomposites with ZA-27 alloy matrix. In: *15th international conference on tribology – SERBIATRIB '17*, Kragujevac, Serbia, 17–19 May 2017, pp.169–176.

39. Saravanan RA, Surappa MK and Pramila Bai BN. Erosion of A356 Al-SiCp composites due to multiple particle impact. *Wear* 1997; 202: 154–164.
40. Miyazaki N and Funakura S. Solid particle erosion behavior of metal matrix composites. *J Compos Mater* 1996; 30: 1670–1682.
41. Ninham AJ and Levy AV. The erosion of carbide-metal composites. *Wear* 1988; 121: 347–361.
42. Wilson S and Ball A. Wear resistance of an aluminium matrix composite. In: *First South African colloquium: the engineering development and application of composite Materials*. Johannesburg, South Africa, 23 July 1990, paper no. 5.
43. Laguna-Camacho JR, Vite-Torres M, Gallardo-Hernández EA, et al. Solid particle erosion on different metallic materials. In: H Pihtili (ed.) *Tribology in engineering*. Rijeka: InTech, 2013, pp.63–78.